Inorganic Chemistry

ARTICLE

pubs.acs.org/IC

Absorption and Fluorescence Spectroscopy of Growing ZnO Quantum Dots: Size and Band Gap Correlation and Evidence of Mobile Trap States

T. Jesper Jacobsson* and Tomas Edvinsson

Department of Materials Chemistry, Uppsala University, Box 538, 75121 Uppsala, Sweden

Supporting Information

ABSTRACT: ZnO nanoparticles constitute a convenient model system for fundamental studies with many possible technical applications in, for example, sensors and the field of catalysis and optoelectronics. A large set of ZnO quantum dots in the size range 2.5−7 nm have been synthesized and analyzed in detail. Time resolved in situ UV−vis absorption measurements were used to monitor the growth of these particles in solution by correlating the optical band gap to particle size given from X-ray diffraction (XRD) measurements. The particles formed were isotropic in shape, but small initial deviations gave indications of a transition from thermodynamic to kinetically controlled growth for particles around 4 nm in diameter. On the basis of this, the behavior and mechanisms for the particle growth are discussed. The fluorescence dependence on particle size was investigated by combining fluorescence and UV−vis measurements on growing particles. This revealed that the positions of the fluorescence trap states are mobile toward the conduction- and valence band. A broadening of the trap states was also found, and a surface dependent mechanism of the trap state shift and broadening is proposed.

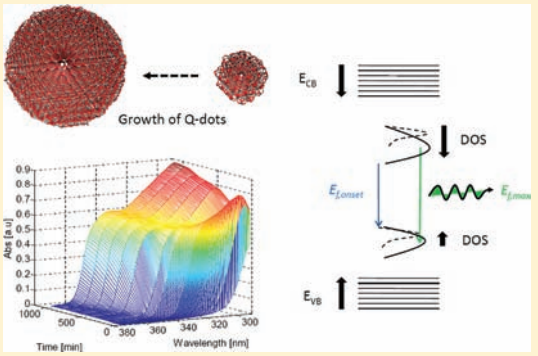

1. INTRODUCTION

ZnO is an interesting material with many possible nanoscale applications in sensors,[1] catalysis,[2] photovoltaics,[3] and spintronics[4] to mention just a few. This is largely due to its many desirable material properties, like a direct band gap, high absorption coefficient, good carrier mobility, ease of doping, and versatile synthesis condition producing both particles, nanorods, and other geometries.[5−8]

In this work we have performed a detailed absorption and fluorescence study of wurtzite ZnO in the quantum confined region, that is, 2−7 nm, with the intention to resolve the optical properties for a very large number of different sizes. Here the semiconductor ZnO nanoparticles are small enough for the exciton levels to be confined within the particles in all three spatial dimensions, thus causing the electronic and optical properties of the particles to change. For the size regime studied, the ZnO particles are small enough to show optical quantum confinement effects, such as a band gap shift, but still large enough to be analyzed with X-ray diffraction (XRD). This also enables us to determine if a change in lattice cell parameters for ZnO quantum dots is an important mechanism for the band gap change. The smallest particles are also small enough for theoretical calculations comparable to experiments, which were done in a parallel study.[9]

We report the buildup of ZnO quantum dots while monitoring how the optical and structural properties changed during the process. A new modified empirical relation between band gap and particle size have been developed, which enabled in situ size determination of growing particles. The fluorescence behavior of the particles was investigated by correlating in situ steady state fluorescence measurements with UV−vis absorption on growing particles in solution. With the extensive data set available, we could resolve details in the size dependent shift of the fluorescence with respect to intensity and wavelength. In particular we find that the fluorescence trap levels are decoupled from the conduction and valence band edge when the particles grow.

The paper starts with a short theory section followed by details about the experimental procedure. The results section starts with a discussion of XRD data for particles with different sizes in relation to UV−vis data. On the basis of this, a correlation between band gap and particle size is made and is further used to give insight into the growth behavior. In the last part, steady state fluorescence from growing particles is reported, and a mechanism of the size dependent shift of the fluorescence is proposed.

2. THEORY

2.1. Correlations between Band Gap and Particle Size. A striking aspect of quantum dots is the size dependence of the optical properties. When a very small semiconductor molecular cluster increases in size, the band gap decreases and the

Received: June 21, 2011
Published: August 29, 2011

absorption edge shifts to longer wavelengths. A simplistic explanation is given within the framework of molecular orbital theory. When particles grow, the energy levels split and eventually transform into dense energy bands in a transformation over molecular and cluster-like orbitals. The broadening of the occupied and unoccupied orbitals thus leads to the observed decrease of the band gap, and eventual convergence to the band gap of the bulk material. To go beyond this simplistic picture to a more quantitative model is not trivial. To do this, different set of assumptions need to be made, and more or less elaborate ways have been described in the literature to separate different regions of quantum confinement.[10] In a first approach made by Brus,[11] the photogenerated electron hole pair is approximated with a model Hamiltonian for a bound state within the effective mass approximation in an effective surrounding potential, given in eq 1.

$$\hat{H} = \frac{-\hbar^2}{2m_e^*}\nabla_e^2 + \frac{-\hbar^2}{2m_h^*}\nabla_h^2 - \frac{e^2}{\varepsilon|r_e - r_h|} + \sum_{n=1}^{\infty} a_n \frac{e^2}{2}\frac{(r_e^{2n} + r_h^{2n})}{R^{2n+1}} \quad (1)$$

Here $\hbar$ is Planck's reduced constant, ε the dielectric constant, α the polarizability, r_e and r_h are the position for the electron and the hole within the particle, R is the particle radius, and m^*_e and m^*_h are the effective masses for the electron and hole, respectively. Following Brus, we can assume that the correlation between the hole and electron is small and that the wave functions for the electrons and holes can be separated as $\Psi = \Phi(\mathbf{r_e})\Phi(\mathbf{r_h})$ giving an additive energy contribution. The last term in eq 1 is the effective polarization which is negligible for large particles where $R \gg r_e + r_h$, and angular independent because of the assumption of isotropic particles. Without the last term the model Hamiltonian reduces to the screened Wannier Hamiltonian for a bound electron-hole pair. The Schrödinger equation is then solved for the first exited state for a particle with radius R within the effective mass approximation for the kinetic energy and a higher frequency dielectric screening approach for the potential energy giving the band gap energy as eq 2.

$$E_g = E_{g,bulk} + \frac{\hbar^2\pi^2}{2R^2}\left(\frac{1}{m_e^*} + \frac{1}{m_h^*}\right) - \frac{1.8e^2}{\varepsilon R} + \frac{e^2}{R}\sum_{n=1}^{\infty}\alpha_n\left(\frac{r_e + r_h}{R}\right)^{2n} \quad (2)$$

Here $E_{g,bulk}$ is the band gap of the bulk material, which is 3.3 eV in our case. The second term is the increased kinetic energy from the localization of the electron−hole pair inside a sphere with radius R and scales as R^{-2}. The third term is the Coloumb attraction in a screened environment and scales as R^{-1}. The polarization term, expressed as an average polarization in eq 2, has the same scaling as the screened Coulomb attraction. This gives a physical motivation for a functional dependence between the band gap, E_g, in eV and the particle diameter, d, in nm as in eq 3, where the coefficients C_n are to be found, and which Brus determines to be 3.37, −1.35, and 8.47.

$$E_g = C_1 + \frac{C_2}{d} + \frac{C_3}{d^2} \quad (3)$$

This model is however claimed to overestimate the size for particles smaller than ∼5 nm[12]. An alternative approach by Viswanatha et al[12] uses the tight binding approximation to calculate the size dependence of the band gap, and also relate E_g to experimentally determined particle sizes from XRD data. This analysis gives better correlation to experimental data, but at the cost of analyticity. The latter approach generates two expressions; eq 4, that resemble the functional dependence of Brus but with variable exponents similar to the cluster size equations from Jortner,[13] and eq 5, representing a good fit to data without any particularly physical motivation for the functional dependence. E_g is given in eV and d in nm.

$$E_g = 3.35 + \frac{1.67}{d^{1.4}} \quad (4)$$

$$E_g = 3.35 + \frac{100}{18.1d^2 + 41.4d - 0.8} \quad (5)$$

A third approach to the problem is a purely experimental one made by Meulenkamp.[14] In that work particle sizes were calculated from XRD data and compared to the wavelength at half the absorption of the first absorption maximum when going from longer wavelengths. This is a value slightly different from E_g but with a similar functional dependence of the particle size. The data was fitted to the functional form of eq 3, and gave the coefficients 3.301, 1.9, and 294. In the following section we will reanalyze the problem with a more extensive set of particle sizes, which should give a more reliable relation.

3. EXPERIMENTAL METHODS

3.1. Synthesis. Two different sets of experiments have been done. In one, particles have been studied during growth in solution. In the other set of experiments particles have been precipitated from the solution at certain times to stop the growth and to make films of quantum dots. A sol−gel like synthesis method originally developed by Spanhel et al.[15] and later refined by Meulenkamp[14] is used with some minor modifications.

In the standard case, 2.5 mmol $Zn(OAc)_2 \cdot 2\ H_2O$ are dissolved in 25 mL of boiling ethanol under vigorous stirring for 1 min. The solution is then cooled in an ice bath, and thereafter mixed with 25 mL of 3.5 mmol $LiOH \cdot H_2O$ ethanol solution. When the two solutions are mixed, ZnO particles begin to grow which can be followed in situ with UV−vis spectroscopy.

This is a simplification compared to the recipe of Meulencamp as $Zn(OAc)_2 \cdot 2\ H_2O$ is used without pretreatment. This makes it possible to within half an hour go from dry chemicals to a solution of growing ZnO nanoparticles.

The particles were washed from unreacted species and acetate salts by adding heptane to the particle solution, which is miscible in ethanol but decreases the solubility of the particles. After addition of heptane, typically three times the volume of the particle solution, the particles agglomerate, and the solution becomes turbid. The particle solution was centrifuged at 5000 rpm to precipitate the particles, and then redispersed in ethanol whereupon subsequent precipitations and washings where possible.

Film deposition was made by dissolving the precipitate after centrifugation after one wash cycle in a small amount of ethanol. Two drops of ethanol are enough to dissolve precipitate from 2.5 mL of washed particle solution. The solution was then ultrasonicated after which it was transferred to the substrate. A smooth, transparent film was then formed after evaporation of the excess solvent. With this method it was possible to produce films with particle diameters down to 2.5 nm in a reproducible way. To be able to directly combine transient absorption measurements of particles in the films with other measurements, amorphous soda lime glass was used as substrate.

dx.doi.org/10.1021/ic201327n |Inorg. Chem. 2011, 50, 9578–9586

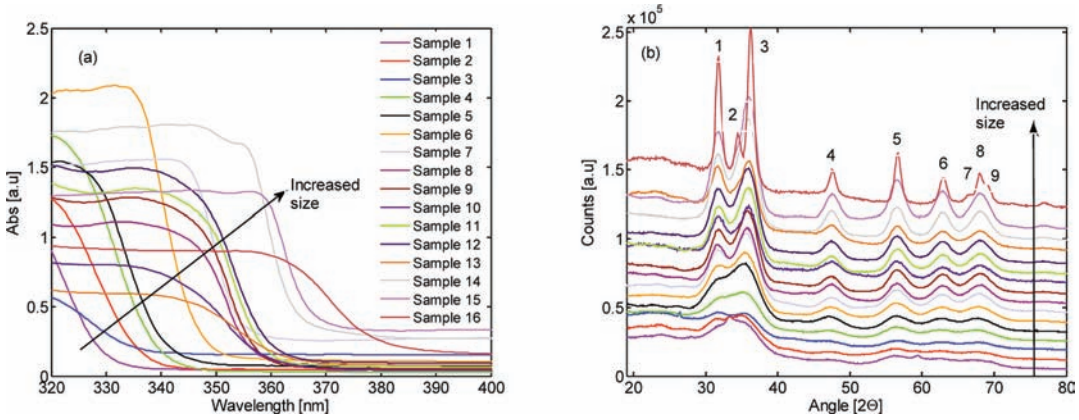

Figure 1. (a) Absorption spectra for the analyzed samples, named in order of increasing band gap. The non uniformity in the absorption intensity is due to differences in film thickness. (b) XRD data for the analyzed samples. The curves are shifted in *y*-direction so that curves for particles with larger band gap (smaller particles) are below curves for particles with smaller band gap. The color settings are the same as in (a).

Table 1. XRD Reference Data and Peak Assignment for Wurtzite ZnO[a] [15]

peak number	2θ	d(Å)	I_n	h	k	l
1	31.7694	2.814300	57	1	0	0
2	34.4211	2.603320	44	0	0	2
3	36.2521	2.475920	100	1	0	1
4	47.5376	1.911140	23	1	0	2
5	56.6015	1.624720	32	1	1	0
6	62.8626	1.477120	29	1	0	3
7	66.3783	1.407150	4	2	0	0
8	67.9608	1.378180	23	1	1	2
9	69.0981	1.358250	11	2	0	1

[a] The cell parameters *a*, *b*, and *c* are 3.250 Å, 3.250 Å, and 5.207 Å, respectively. I_n is normalized intensity.

3.2. Characterization Methods. XRD measurements were performed with a Siemens D5000 Diffractometer using parallel beam geometry with X-ray mirror and parallel plate collimator of 0.4°. Cu Kα with a wavelength of 1.54 Å was used as X-ray source. The angle of incidence was 0.5°, and 2Θ scans were performed between 10° and 90° with a step size of 0.1°. The UV−vis absorption measurements were performed on an Ocean Optics spectrophotometer HR-2000 γ with deuterium and halogen lamps. In all measurements, a full spectrum from 190 to 1100 nm with 2048 evenly distributed points was sampled. To obtain good statistics an average over 100 consecutive spectra as well as for each four consecutive measurement points were done.

Steady state fluorescence was measured on a SPEX Fluorolog II. Particle solution was prepared according to the standard procedure and thereafter diluted by a factor 20 after 2 min. The measurements were started within 5 min after the dilution, and were performed for 30 h. The excitation wavelength was 320 nm, and the fluorescence was measured between 330 and 720 nm. A filter was used to attenuate a large part of the signal for wavelengths longer than 660 nm. To correlate the fluorescence behavior to particle size, UV−vis spectroscopy was measured simultaneously as the fluorescence.

4. RESULTS AND DISCUSSION

4.1. XRD. XRD were measured on 16 samples in total, in the form of quantum dot particle films deposited on transparent amorphous glass substrates. The substrates were chosen to perform absorption measurements on the samples under the same conditions as the XRD measurements, and by this having full control over possible particle growth during the measurement procedure. In Figure 1a the absorption data for all the samples are displayed, named in order of increasing band gap calculated as outlined in the Supporting Information. The corresponding diffractograms are displayed in Figure 1b.

The sample with largest particles and thus least peak broadening showed nine distinct peaks. Besides these peaks, a few other distinct features of the diffractogram were present. Most notably was a large diffuse signal between 20° and 30° and a high background, especially at low angles, because of the amorphous glass substrate. All the observed peaks correspond to the diffraction data for wurtzite ZnO,[16] given in Table 1.

For the smaller particles the peak broadening was large, and some of the peaks overlap substantially. The smaller particles also gave a weaker signal, making the measurement more sensitive to noise and background signal. Two of the measurements with the smallest ZnO particles show a few additional small peaks that may be attributed to remaining crystalline acetate species. The XRD data show that the remaining films contain crystalline wurtzite ZnO particles, and no measurable amounts of other crystalline species. This was also verified by Raman measurements.[9]

The particle size is estimated with the peak broadening using the method of Scherrer,[17] which is considered a standard method. The sizes determined by XRD are strictly not particle size but the size of the crystal grains, and do not take into account possible amorphous surface layers. TEM results from other groups[12,14] using this synthesis method have however shown that the size from XRD is consistent with the size from TEM, and that the particles constitute of single crystal grains. The good agreement with the expected diffraction data of wurtzite ZnO and our particles and the gradual development of the peaks as the particles grows support this. XRD also have the benefit over TEM in that it gives the volume average size which is directly comparable to the volume cross section obtained in optical absorption measurements, and not the number average as obtained in TEM.

All XRD-peaks are however not well suited for size determination, which demands that some care is taken when analyzing the data. Details of this are described in the Supporting Information,

dx.doi.org/10.1021/ic201327n |*Inorg. Chem.* 2011, 50, 9578–9586

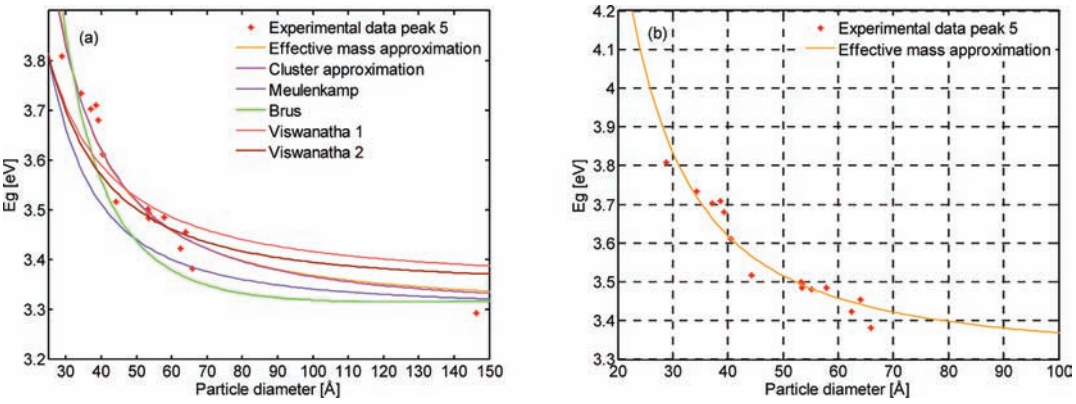

Figure 2. Band gap against particle sizes for peak 5 (56.6°) together with (a) expressions from the literature and, together with (b) the best fit according to eq 6 that are used for determination of particle sizes in this work.

but in short the data for peak 5 (56.6°) and 6 (62.9°) gives the most reliably data as the problem of peak overlap and background compensation is smallest for theses peaks.

It should be noticed that peak broadening can be caused by strain as well as by small size. One way to separate the contributions from stress and strain is by the Williamson-Hall method. A drawback with that method is that it demands good data for both high and low angle reflexes, which is problematic in our case because of the large peak overlap at high angles and background removal at low angles. The Williamson-Hall method is therefore not applicable in our case and no information about the stress in the particles is available. It is however reasonable to assume that the broadening due to strain is small, as the particles and their surfaces subjected to growth easily should be able to relax when free in solution.

A size determination has been done with data from peak 5 (56.6°) as well as for peak 6 (62.9°), and this data are fitted to expressions of the form of the Brus effective mass approximation,[11] eq 1, as well as to Jortner's cluster equation.[13] The results for peak 5 (56.6°) are stated in eq 6 and 7, as well as in Figure 2a. The two expressions give more or less identical results in the experimental range, and when particle sizes have been calculated from absorption data eq 6 is the one that have been used. This is plotted in a clear way in Figure 2b.

$$E_g = 3.30 + \frac{0.293}{d} + \frac{3.94}{d^2} \quad (6)$$

$$E_g = 3.30 + \frac{3.54}{d^{1.73}} \quad (7)$$

In Figure 2a experimental data for peak 5 (56.6°) are plotted together with the expressions from the literature given in section 2.1 and the fitted expressions in eq 6−7. Our expression is based on a considerably larger set of particle sizes than other relations found in the literature, and as more concern has been put on the analysis of the XRD data than normally is the case,[12,14,18] it should constitute the best empirical relation available between optical band gap and particle size. It is also valid for the smallest particles in the most quantum confined region. Corresponding figures for peak 6 (62.9°) are found in the Supporting Information.

When the particle size decreases below 3 nm the change of the band gap is rather dramatic. Extrapolating into this regime is therefore difficult and bound to have a large degree of uncertainty. Departing from the experimental data and performing an estimation from the effective mass model is problematic as well in this region since the effective masses have not been unambiguously determined. The effective electron mass in ZnO, for example, has been reported between 0.24 and 0.30[11,19] giving a non negligible difference in the band gap shift within this model. Neglecting polarization in eq 2 (independent of effective mass) and using $\varepsilon = 3.7$, $m_h^* = 0.45$, and $m_e^* = 0.30$ for wurtzite ZnO one obtains a band gap shift of 0.45 eV for a quantum dot with 3 nm in diameter. Using $m_e^* = 0.24$ instead gives a 0.59 eV band gap shift. An estimation from the effective mass is also complicated because of the uncertainty in the effective mass for the hole, which has been reported up to $m_h^* = 0.6$[20,21]

For really small particles there are some theoretical band gap calculation reported. For the assumed precursor molecule, basic zinc acetate, with a diameter around 0.32 nm, first principles calculations give the energy difference between the highest occupied molecular orbital (HOMO) and the lowest unoccupied molecular orbital (LUMO) equal to 5.74 eV.[22] Further on Spanhel[5] suggests values of the first excitation energy {5.74, 5.39, 4.51, 3.87 eV} for some smaller particles with a diameter of 0.323, 0.64, 1.28, and 2.56 nm. The accuracy of these calculations is not addressed, but nevertheless, the calculations do not capture the behavior in any of the expressions in Figure 2a. The idea of capturing the size dependence of the band gap with only a second degree polynomial may be a somewhat naive approach but nevertheless it turns out to be a very a useful approach for particle size determination in experimental work.

Peak 5 (56.6°) represent the most reliable part of the XRD data, but does not contain information about the extension in the *c*-direction, as it is caused by the [1 1 0] reflection. For spherical particles this does not matter, but peak 5 (56.6°) data will not capture a possible elongation along the *c*-axis. This cannot be excluded as growth along the *c*-axis normally is more energetically favorable as the surface energy often is higher for the polar surfaces perpendicular to it. To investigate if this is the case, data from peak 5 (56.6°) are compared with data from peak 6 (62.9°) representing the [1 0 3] reflection, which are shown in Figure 3. The two fitted curves cross for particle diameters around 4 nm indicating a slight size dependent deviation from spherical shape. They seems to be slightly elongated along the *c*-axis while less than 4 nm, and elongated along the *a*-axis when larger. The deviation from spherical geometry is rather small, and would also be hard to evaluate with other methods, for example, transmission electron microscopy (TEM) with its problem with statistics and assignment of crystallographic directions for large number of

dx.doi.org/10.1021/ic201327n |*Inorg. Chem.* 2011, 50, 9578–9586

particles. This deviation does, however, indicate that the growth initially is thermodynamically controlled and preferably occurs at the polar surface along the *c*-axis, to later develop into kinetically controlled growth. The degree of kinetic control should, however, be at least of the same order of magnitude as that of the thermodynamic control even for the smallest particles.

A question of interest is whatever or not the lattice cell parameters change with particle size, which in that case could change the band gap because of a different mechanism than the quantization confinement described earlier. For a small particle, a large part of the atoms are located close to the surface, and will have fewer neighbors to bind to compare to the corresponding bulk atoms. This relaxation can go on for several atomic planes, and for a 3 nm large particle most of the atoms are located only a few atom layers from the surface. A reasonable hypothesis is that the average atomic distances, or the lattice cell parameters, would increase slightly when the particle size decreases. From Bragg's law it is evident that a larger spacing between the lattice planes means smaller diffraction angle, and for a hexagonal system, like wurtzite, the relation between the lattice spacing, *d*, the miller indices *h*, *k*, *l* and the cell axis *a*, and *c* are given by eq[23] 8.

$$\frac{1}{d^2} = \frac{4}{3}\left(\frac{h^2 + hk + k^2}{a^2}\right) + \frac{l^2}{c^2} \qquad (8)$$

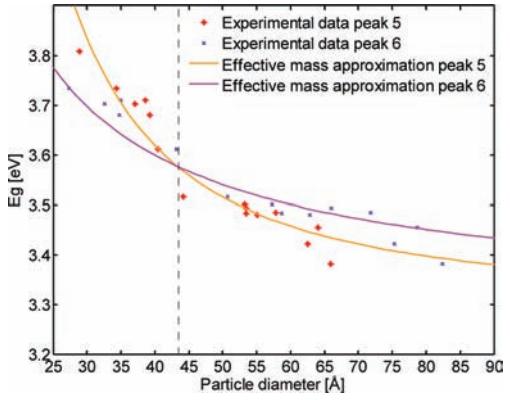

Figure 3. Band gap from absorption measurements versus particle diameter from XRD for reflex 5 (56.6°) and 6 (62.9°), together with fitted expressions from eq 6 for peak 5(56.6°) and the corresponding expression for peak 6 (62.9°) ($3.30 + 1.22/d - 0.0845/d^2$).

Analysis of the diffraction peak positions were made to see if there is such an effect for the studied particles. A weak trend was seen in this direction for data from peak 5 (56.6°), but data scatter a bit and the resolution of the measurement is in the order of 0.1° wherefore a detailed analysis not has been possible. Data do however bound the cell elongation along the *a*-axis to be less than 0.2% or 3×10^{-13} m while decreasing the diameter from 14 to 3 nm. We can thus conclude that an effective increase in the cell parameters not is likely to play a major part in the observed band gap shift for small ZnO particles.

4.2. UV−vis Spectroscopy and in Situ Growth Studies. UV−vis spectroscopy was employed for time-resolved in situ measurements on growing particles in solution, allowing the quantum confinement to be studied in detail during growth. Absorption as a function of wavelength and time for the first 18 h after initiation is given in Figure 4a, for synthesis according to the standard procedure but diluted by a factor five. The first absorption maximum when going from lower energies, corresponding to the ridge at higher wavelengths, is given as a function of time in Figure 4b. By knowing the absorption coefficient, it is possible to estimate the fraction of the reactants that have reacted and formed particles. See Supporting Information for details.

The absorption in Figure 4 show a fast initial increase, passes through a maximum and then levels off. This indicates a fast initial nucleation and growth phase during the first minutes, followed by a stabilization of the total amount of reacted species. During this period the particles reach approximately 2.5 nm in diameter. It is also apparent that a rather large part of the reactants relatively fast are accounted for in the form of particles. This validates the assumption that the particles consist of single crystals, as the absorption profile is consistent with small wurtzite ZnO particles. The method for determining the degree of reaction does actually only take into account the largest particles, and the slight decrease in this parameter with time can be interpreted as a development of a slight polydispersity. The amount of reactants accounted for in the largest particles, however, does not allow more than a small polydispersity. This is in line with TEM data[14] which states that 85−90% of the particles have a size within 20% of the mean diameter for this synthesis method.

The observations may be explained as follows. The initial conditions favor nucleation and some initial growth whereupon many small and slightly larger nuclei are formed. As the reaction

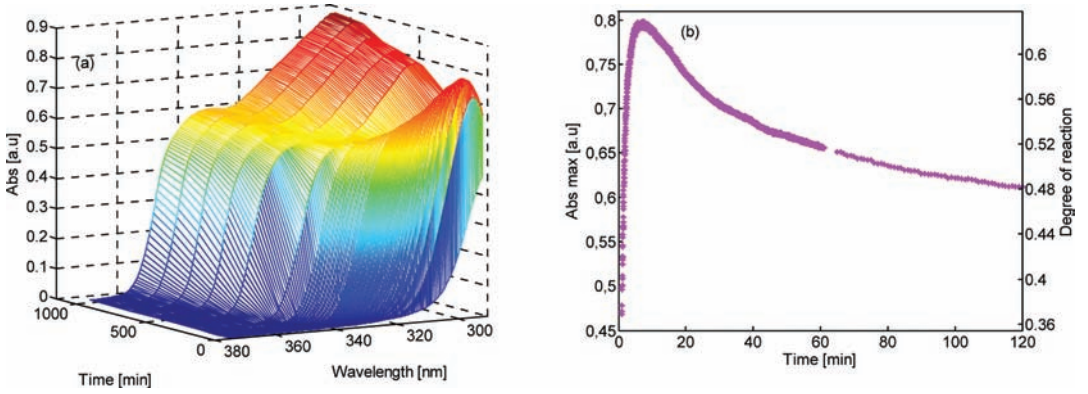

Figure 4. (a) Absorption as a function of wavelength and time during the first 18 h after mixing of the reagents. The diameter of the particles increases from 2.5 to 5.5 nm. (b) Absorption at the first maximum when going from higher wavelengths, and degree of reaction as a function of time. The absorption corresponds to the ridge at higher wavelengths in (a).

dx.doi.org/10.1021/ic201327n |*Inorg. Chem.* 2011, 50, 9578–9586

proceeds there are some changes in the reaction conditions making the nucleation less favorable. This can be attributed to a pH decrease because of OH^- consumption and depletion of reactants. The larger nuclei then grow while the smaller ones dissolve, explaining that particles grow simultaneous as the overall amount of solid substance in the solution stabilizes. This is based on the principle that the surface tension, or energy, increases with increased curvature and therefore favors dissolution for smaller particles. When the concentration of reaction species decreases in the solution smaller particles will dissolve while larger ones continue to grow. In Figure 4a there are two ridges evolving, where one can be attributed to larger growing particles and the other one for smaller dissolving particles, supporting the reasoning.

To investigate this further, absorption measurements have been done on samples with different initial concentrations of reactants, and from these measurements it is seen that the initial pH and reactant composition has a large effect on the particle growth (see Supporting Information for details). If the initial pH is too high no particle growth will occur, and if it is slightly too low only a few particles will grow, which consumes OH^-, until the pH reaches a critical level where no further nucleation and growth is occurring. The effect of dilution is however rather small and insignificant in comparison to the effect of the $Zn(OAc)_2$: LiOH ratio, illustrating that the relative proportion of reagents are more important than their absolute concentrations.

In both the methods of Spanhel et al.[15] and Meulenkamp,[14] on which the present approach is based, $Zn(OAc)_2 \cdot 2\,H_2O$ is boiled with the solvent during a shorter or longer time. It has been conjectured that this step is necessary for the formation of the initial clusters, presumably basic zinc acetate,[2] $Zn_4O(OAc)_6$. Experiment where $Zn(OAc)_2 \cdot 2\,H_2O$ and LiOH were mixed in cold ethanol show the same absorption behavior as samples that have undergone heat treatment. The conclusion is that formation of the initial clusters is not an activated process demanding elevated temperature, and that the heating step is not necessary. Heat treatment is, however, beneficial in the sense that it facilitates the solvation of the zinc salt.

The mechanism by which the particles grow is not completely clear. One approach to an explanation is made by Wong et al.,[24] who have studied growth kinetics of ZnO particles synthesized from $Zn(OAc)_2 \cdot 2H_2O$ with NaOH as base and 2-propanol as solvent. There, an approach with the Lifshitz−Slyozov−Wagner theory, LSW, for Ostwald ripening is suggested to describe the particle growth. A theoretical treatment of the problem leads to eq 9, where the cube of the particle radius, r, is proportional to time, t. K is a proportionality constant and r_0 the particle radius at time zero. This means that a plot of particle volume against time should generate a straight line, which also is what Wong et al[24] seem to obtain.

$$r^3 = r_0^3 + Kt \tag{9}$$

Such a plot for our data is given in Figure 5. A clear deviation from linear behavior is seen, suggesting that the growth mechanism is more complex than simple Ostwald ripening. A difference between our data and Wong's is that they have rather few data points for every composition, while we have several thousands, and thereby a possibility to do a more certain evaluation.

A growth mechanism beyond simple Ostwald ripening is proposed by Spanhel et al.[5,15] which suggests that growth may be due to aggregation of small clusters into larger ones by coalescence.

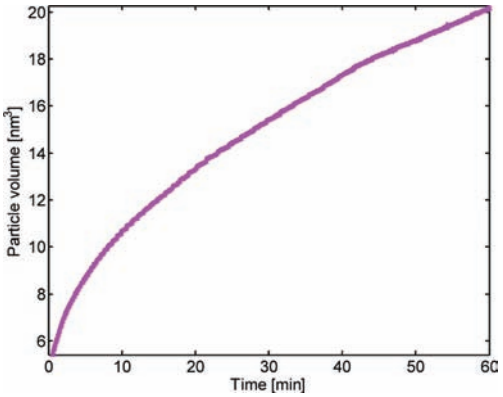

Figure 5. Particle volume as a function of time. It is clearly seen that the relation not is linear.

In favor for a mechanism of this kind is that no particles smaller than ∼2.5 nm are observed in the absorption measurements, which could represent the fourth discrete cluster described by Spanhel.[5] Something that disfavors this kind of mechanism is that it implies that certain sizes should be more stable than others and therefore also more abundant or long-lived. This is something that not is seen in our absorption measurements, where a smooth continuous growth is observed which is rather the opposite behavior. This mechanism is thus unlikely, at least for particles with a diameter over 2.5 nm.

On the basis of the experimental data, we propose the following general scheme for ZnO particle nucleation and growth under the conditions studied. Initial nucleation does not demand heat, but a certain OH^- concentration. If the OH^- concentration is too low, no nucleation is occurring, and if too high it will slow it down because of less likelihood of breaking the $Zn(OAc)_2$ complex. After, or simultaneously as the nucleation, a rather fast growth of particles is occurring, and these two steps will consume OH^-. This will depress any further nucleation and slow down the hydrolysis of the particle surfaces. The larger particles will then continue to grow but at a slower rate, at the same time as the smaller particles dissolve. This is occurring in an Ostwald like process, even if the complexity of the system does not enable a straightforward use of the theory. To resolve more of the optical properties of growing ZnO nanoparticles, the fluorescence behavior was monitored during growth which is described below.

4.3. Steady State Fluorescence. Time resolved in situ steady state fluorescence measurements were performed on growing particles in solution simultaneously with absorption measurements. In Figure 6a, the fluorescence is given as a function of time and wavelength. The band gaps for the particles are determined from simultaneous absorption measurements and given in Figure 6b. Particle sizes are given by eq 6, and are together with the band gap plotted as a function of time in Figure 6c.

The fluorescence in Figure 6a shows a strong signal in the greenish region around 550 nm. Also a weaker UV-fluorescence with energy slightly below the band gap is reported in the literature[25,26] and can be noticed in the data. It is much weaker than the strong visible fluorescence and not discussed further.

The exact origin of the visible fluorescence is still elusive and there is so far no unambiguous mechanism for the green emission. The emission has been assigned to defects originating in Zn vacancies,[27] Zn interstitials,[28] antisite oxygen,[29] oxygen

dx.doi.org/10.1021/ic201327n |Inorg. Chem. 2011, 50, 9578–9586

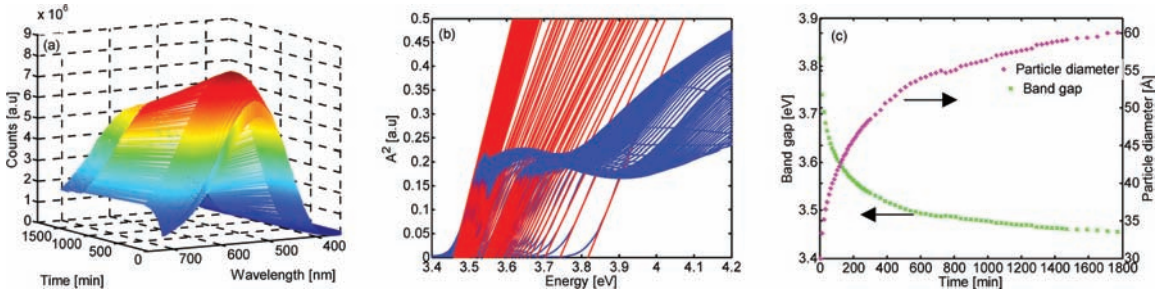

Figure 6. (a) Steady state fluorescence as a function of wavelength and time for 30 h after mixing of the reagents. (b) Determination of E_g from absorption measurements corresponding to the fluorescence measurements in (a), by assuming parabolic bands close to the band edges as described in the Supporting Information. (c) Band gap (green crosses) and particle diameter (purple asterisks) as a function of time.

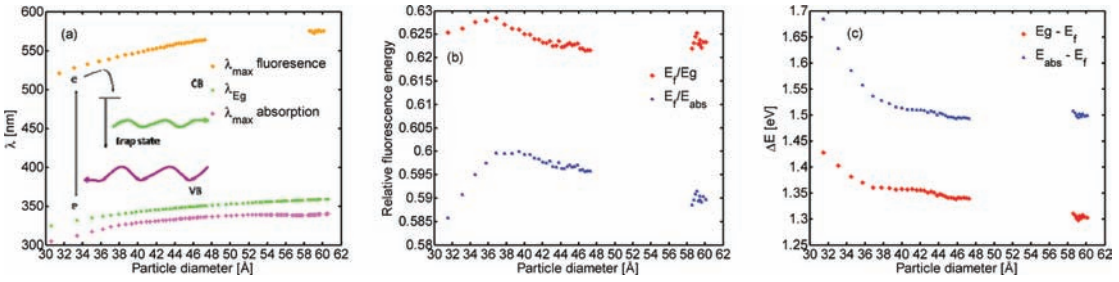

Figure 7. (a) Wavelength for the first absorption maximum when going from longer wavelengths, wavelength for the fluorescence maximum, and the wavelength corresponding to the band gap energy, as a function of particle diameter. The inset illustrates the energy levels involved. (b) Relative fluorescence energy between the band gap energy, and between the maximum absorption energy. (c) Difference in energy between the band gap and the fluorescence energy at maximum fluorescence intensity, and the difference in energy between the absorption and the fluorescence energy at maximum intensity. These data are given as a function of reaction time in the Supporting Information.

vacancies,[30] and Cu impurities[31]. One of the difficulties is that the Zn and O vacancies are hard to distinguish and that many of the experiments involve perturbations affecting both the Zn and the O properties. The Zn vacancy hypothesis, for example, is supported by Zn and O implantation[32] while also the O content at the surface can be affected by Zn implantation because of preferential sputtering and different ion backscattering. The methods, however, have minor effects on the Cu content and thus imply that the intrinsic Cu impurities in the Zn precursors are not any major contributors to the green emission in general. One strong support for the O vacancy hypothesis with minor effect on the Zn vacancies is the enhancement of the green emission when annealing above 600 °C and thus enforce out-diffusion of oxygen.[33] A suggested mechanism in the literature is radiative recombination of electrons populating levels close to the conduction band edge down to a deeply trapped hole of $V_O^{\bullet\bullet}$ type in the bulk of the ZnO particle.[25] Although there is no fully conclusive evidence of the type of defect that is the origin of the green emission, there is growing evidence that the defects are located at the surface.

The fluorescence intensity in Figure 6a increases initially after which it reaches a maximum and then steadily decreases. This fluorescence maximum has been observed in the literature[34] as well as the decrease of fluorescence intensity with increased particle size.[22,35,36] This behavior can be rationalized by the availability of surface states. At the beginning of the synthesis the total amount of ZnO surface increases as particles nucleate and grow. After a while the maximum absorption is stabilized, implicating that the amount of solid ZnO remains constant. Larger particles will then grow at the expense of the smaller ones that are dissolved, and thereby decrease the total amount of surface in the system.

Close to the surface, the numbers of defects are larger than in the bulk, as the number of irregularities, dangling bonds, and degree of unsaturated coordination are larger there. If the fluorescence depends on trap states associated with the particle surface, it is likely that the fluorescence should decrease with time under the experimental conditions used. This can be seen in Figure 6a, including a short increase in the beginning when the amount of surface area is increasing, and thereby confirming the picture that the visible fluorescence is strongly dependent on surface states. Explanations in the literature are similar in that they ascribe a large importance to the surface properties of the particles, like the presence of O^{2-} ions at the particle surface,[27] stabilization by acetate groups,[26] or F-centers close to the surface.

In Figure 7a the wavelength at the maximum fluorescence, the first absorption maximum when going from longer wavelengths, as well as the wavelength corresponding to the band gap, is displayed as a function of particle size. The fluorescence is shifted to longer wavelengths with increasing particle size, which is not surprising. When the particles grow, the band gap decreases, and it is not strange that the energy difference between two trap levels within the band gap decreases as well. This is also in good agreement to what is reported in the literature.[22,34,35,37]

More interesting is the way this decrease occurs. In Figure 7b the relative fluorescence energy between the band gap energy and the energy at maximum absorption intensity are plotted as a function of particle size. Here we can note a small initial increase in relative energy followed by a maximum at a particle size corresponding to around 4 nm and then a slow decrease of fluorescence.

The fluorescence energy is fairly constant around 62.5 ± 0.4% of the band gap energy and 59.2 ± 0.8% of the energy at

dx.doi.org/10.1021/ic201327n |*Inorg. Chem.* 2011, 50, 9578–9586

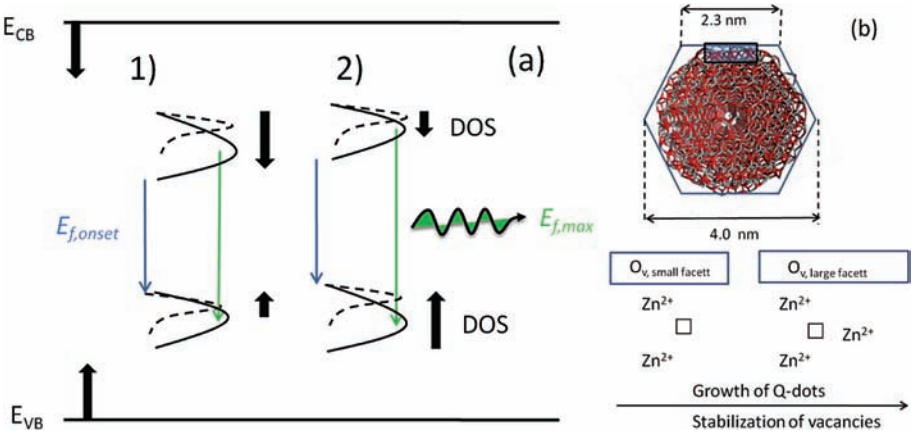

Figure 8. (a) Schematic illustration of the relative trap movement and density of states (DOS) broadening with (1) slower decrease of the lower trap state compared to the valence band edge and (2) slower decrease of the upper trap states compared to the conduction band edge. The maximum fluorescence intensity, $E_{f,max}$, is depicted from the maximum DOS in the donor states to the maximum DOS in the acceptor states. (b) A 4 nm ZnO quantum dot is depicted with the facet size and the (001) surface marked. The structure is from a reactive force field calculation performed in a separate study.[9] As the ZnO quantum dots grow, the facets become larger and the idealized curvature becomes less, which leads to a larger fraction of coordinated vacancies.

maximum absorption. The rather constant values show that when the particles grow there is close to a linear contraction of the band gap and the energy levels within it after some initial surface reconstruction. In Figure 7c the energy difference between the fluorescence energy at maximum fluorescence intensity and both the band gap and the maximum intensity of the absorption are plotted. From the figure it is apparent that the energy differences between the maxima decreases when the particles grow in the beginning of the synthesis to level off to a rather constant value. The energy difference between the two fluorescence trap states then decreases slower with particle size than the band gap does. This means that the fluorescence trap levels cannot be fixed relative to the conduction band (or to the valence band) for particles smaller than 4 nm, as that should lead to a constant energy difference.

The fluorescence trapping levels are likely to be affected by properties of the particle surface, which change as the particle size and synthesis conditions change with time. The pH value is likely to decrease during the synthesis, which in turn would lead to less negatively charged surfaces. This would lead to a destabilization of the lower hole trap states situated at or close to the surface. This would in turn decrease the fluorescence energy as the distance between the lower trap state and the valence band should increase, and thereby decouple the density of trap levels from the valence band and enable the effective contraction between the fluorescence trap levels. The same reasoning would give a decoupling between the charge stabilized higher trap states and the conduction band. The observed behavior in Figure 7c, however, shows exactly the opposite behavior. The gap between the upper and lower trap state is decreasing slower than the optical band gap. This implies that geometric factors for trap stabilization dominate over differences in surface charges. We also find that *the onset* of fluorescence changes slower with particle size compared to the energy of the fluorescence maximum (see Supporting Information). This shows that besides the decoupling of the trap states from the conduction and valence band energies, the density of trap states is broadened during particle growth. A graphical representation of this can be seen in Figure 8a.

Note that the green emission can also originate in donor states of singly charged oxygen vacancies to acceptor states below the valence band and that Figure 8a is only a rationalization of the trap movement and broadening without specific determination of their absolute position. On the basis of the fluorescence data above, we propose the following general surface stabilization mechanism. As the ZnO particles grow, the curvature of the surface becomes lower, and facets become larger. This decrease the number of edge vacancies and successively larger fraction of more stabilized vacancies at the surface are formed as the particles grow. See Figure 8b. This stabilizes the surface vacancies and lowers the trap energies and would thus counteract the shrinking band gap effect and explain the observed slower shrinking of the energy between the trap states. In addition, one would expect Zn- and O- species at the surface to be in different positions compared to their ideal crystalline positions and would then constitute a form of pseudo-interstitials and form trap states with somewhat different energies. This together with the intrinsic state broadening as the crystal grows would then explain the trap state broadening. The size where the trap state energy differences begin to level off with the optical band gap is for particles of approximately 4 nm diameter. It is interesting to note that this seems to coincide with the transformation from thermodynamic growth to kinetic growth as indicated by the XRD data.

5. SUMMARY AND CONCLUSION

Growing ZnO particles have been analyzed in solution as well as in the form of thin films on glass substrates. By combining particle size, as extracted from XRD data, with band gap given from absorption measurements, a relation between these two properties has been developed and compared with similar relations in the literature but here with a considerably larger data set.

XRD data shows that the particles are isotropic in shape, but indicate that there is a slightly size dependent geometrical asymmetry, with a transition point around 4 nm. This further indicates that the particle growth initially is thermodynamically controlled to later develop into kinetically controlled. The degree of kinetic control should, however, be at least of the same order of magnitude as the thermodynamic control even for the smallest particles. There may be an elongation in the cell parameters for

dx.doi.org/10.1021/ic201327n |*Inorg. Chem.* 2011, 50, 9578–9586

the smallest particles, but the data bounds it to be less than 0.2% or 3×10^{-13} m when going from a 3 to a 14 nm particle. An increase in lattice parameters is thus not a mechanism for band gap increase as ZnO particles get small.

Time resolved in situ absorption measurements was employed to investigate the growth dynamics. The data show that the initial proportions of reagents are of large importance for the particle growth and to which extent they form. In the standard case the nucleation and initial growth are rather fast processes working in the time scale of minutes. Thereafter the total amount of solid substance is fairly constant or decreases somewhat indicating that small particles dissolve as the larger ones grow. On the basis of the experimental results, we have proposed a scheme for the particle nucleation and growth.

The fluorescence measurements show that the visible fluorescence is shifted to longer wavelengths as the particles grow, and that the intensity is closely related to the amount of available surface in the system. The data gives that the energy difference between the fluorescence and the absorption maxima decreases when the particles grow, but that the relative fluorescence energy compared to the band gap energy is fairly constant. This means that the densities of states of the fluorescence trap levels are decoupled relative to the conduction and the valence band. These dynamics of the trap states are attributed to stabilization of surface states and surface properties that change during the synthesis.

■ ASSOCIATED CONTENT

Ⓢ Supporting Information. A description of how the band gap and the degree of reaction is determined from absorption measurements. A more in-depth discussion of the XRD data, including a pictorial presentation of the peak fitting and background removal procedure. Peak angle against particle diameter calculated from XRD peak 5 (56.5°). Peak 6 (62.9°) data plotted as in Figure 2a. Calculated band gaps for the samples analyzed with XRD. Additional data and absorption Figures for sample 1−5 in section 4.2. Particle diameter as a function of time for sample 1−5 in section 4.2. Additionally there is absorption data for the fluorescence samples, a 2D version of Figure 6a and fluorescence onset as a function of time, compared to maximum fluorescence. The data in Figure 7 is given as a function of reaction time. This material is available free of charge via the Internet at http://pubs.acs.org.

■ AUTHOR INFORMATION

Corresponding Author

*E-mail: jesper.jacobsson@mkem.uu.se. Phone: +46 (0)18-4713774. Fax: +46 (0)70-5745116.

■ REFERENCES

(1) Wang, Z. L. *J. Phys.: Condens. Matter.* **2004**, *16*, R829–858.
(2) Wöll, C. *Prog. Surf. Sci.* **2007**, *82*, 55–120.
(3) Quintana, M.; Edvinsson, T.; Hagfeldt, A.; Boschloo, G. *J. Phys. Chem. C* **2007**, *111*, 1035–1041.
(4) Klingshirn, C. *Phys. Status Solidi B* **2007**, *244*, 3027–3073.
(5) Spanhel, L. *J. Sol-Gel Sci. Technol.* **2006**, *39*, 7–24.
(6) Singh, S.; Thiyagarajan, P.; Kant, K. M.; Anita, D.; Thirupathiah, S.; Rama, N.; Tiwar, B.; Kottaisamy, M.; Rao, M. S. R. *J. Phys. D: Appl. Phys.* **2007**, *40*, 6312–6327.
(7) Pacholski, C.; Kornowski, A.; Weller, H. *Angew. Chem., Int. Ed.* **2002**, *41*, 1188–1191.
(8) Tian, Z. R.; Voigt, J. A.; Liu, J.; Mckenzie, B.; Mcdermott, M. J.; Rodriguez, M. A.; Konishi, H.; Xu, H. *Nat. Mater.* **2003**, *2*, 821–826.
(9) Raymand, D. Surface and interface Studies of ZnO using Reactive Dynamics Simulations. Ph.D. Thesis, Uppsala University, Uppsala, Sweden, 2010, ISBN 978-91-554-7857-5.
(10) Fonoberov, V, A.; Balandin, A, A. *Phys. Rev. B.* **2004**, *70*, 195410.
(11) Brus, L. E. *J. Chem. Phys.* **1984**, *80*, 4403–4409.
(12) Viswanatha, R.; Sapra, S.; Satpati, B.; Satyam, P. V.; Dev, B. N.; Sarma, D. D. *J. Mater. Chem.* **2004**, *14*, 661–668.
(13) Jortner, J. *Z. Phys. D: At., Mol. Clusters* **1992**, *24*, 247–275.
(14) Meulenkamp, E. A. *J. Phys. Chem B.* **1998**, *102*, 5566–5572.
(15) Spanhel, L.; Anderson, M. A. *J. Am. Chem. Soc.* **1991**, *113*, 2826–2833.
(16) McMurdie, H.; Morris, M.; Evans, E.; Paretzkin, B.; Wong-Ng, W.; Ettlinger, L.; Hubbard, C. *Powder Diffr.* **1986**, *1*, 76.
(17) Scherrer, P. *Göttinger Nachr. Ges.* **1918**, *2*, 98.
(18) Vargas-Florencia, D.; Edvinsson, T.; Hagfeldt, A.; Furo, I. *J. Phys. Chem. C* **2007**, *111*, 7605–7611.
(19) Tang, H.; Prasad, R.; Sanjinbs, R.; Schmid, P. E.; Lévy, F. *J. Appl. Phys.* **1994**, *75*, 2042.
(20) Syrbu, N. N.; Tiginyanu, I. M.; Zalamai, V. V.; Ursaki, V. V.; Rusu, E. V. *Phys B* **2004**, *353*, 111–115.
(21) Enright, B.; Fitzmaurice, D. *J. Phys. Chem.* **1996**, *100*, 1027–1035.
(22) Bertoncello, R.; Bettinelli, M.; Casarin, M.; Gulino, A.; Tondello, E.; Vittadini, A. *Inorg. Chem.* **1992**, *31*, 1558–1565.
(23) West, A. R. *Basic Solid State Chemistry*, 2nd ed.; John Wiley & sons: New York, 1999; ISBN 10: 0-471-98756-5.
(24) Wong, E. M.; Bonevich, J. E.; Searson, P. C. *J. Phys. Chem. B* **1998**, *102*, 7770–7775.
(25) van Dijken, A.; Meulenkamp, E. A.; Vanmaekelbergh, D.; Meijerink, A. *J. Lumin.* **2000**, *87−90*, 454–456.
(26) Fonoberov, V.; Balandin., A. *Appl. Phys. Lett.* **2004**, *85*, 5971–5973.
(27) Mahan, G. D. *J. Appl. Phys.* **1983**, *5*, 3825–3832.
(28) Korsunska, N. O.; Borkovska, L. V.; Bulakh, B. M.; Khomenkova, L. Y.; Kushnirenko, V. I.; Markevich, I. V. *J. Lumin.* **2003**, *102*, 733–736.
(29) Lin, B. X.; Fu, Z. X.; Jia, Y. B. *Appl. Phys. Lett.* **2001**, *79*, 943–945.
(30) Vanheusden, K.; Seager, C. H.; Warren, W. L.; Tallant, D. R.; Voigt, J. A. *Appl. Phys. Lett.* **1996**, *68*, 403–405.
(31) Garces, N. Y.; Wang, L.; Bail, L.; Giles, N. C.; Halliburton, L. E.; Cantwell, G. *Appl. Phys. Lett.* **2002**, *81*, 622–624.
(32) Zhao, Q. X.; Klason, P.; Willander, M.; Zhong, H. M.; Lu, W.; Yang, J. H. *Appl. Phys. Lett.* **2005**, *87*, 211912.
(33) Meng, X. Q.; Shen, D. Z.; Zhang, J. Y.; Zhao, D. X.; Lu, Y. M.; Dong, L.; Zhang, Z. Z.; Liu, Y. C.; Fan, X. W. *Solid State Commun.* **2005**, *135*, 179–182.
(34) Bahnemann, D. W.; Kormann, C.; Hoffmann, M. R. *J. Phys. Chem.* **1987**, *91*, 3789–3798.
(35) Koch, U.; Fojtic, A.; Weller, H.; Henglein, A. *Chem. Phys. Lett.* **1985**, *122*, 505–510.
(36) Sakohara, S.; Ishida, M.; Anderson, M. A. *J. Phys. Chem. B* **1998**, *102*, 10169–10175.
(37) Fonoberov, V.; Balandin., A. *Phys. Rev. B* **2006**, *73*, 165317.